Progress In Electromagnetics Research C, Vol. 144, 181-188, 2024

PIER C

(Received 27 March 2024, Accepted 14 June 2024, Scheduled 29 June 2024)

Design of Miniaturized Dual Band-Pass Filter for ISM and Sub-6 GHz Spectrum by Employing Square Complementary Split Ring Resonator

Thupalli Shaik Mahammed Basha[1,2,*], Arun Raaza[1], Vishakha Bhujbal[3], and Mathivanan Meena[1]

[1]*Department of Electronics and Communication Engineering, Vels Institute of Science, Technology & Advanced Studies (VISTAS) Chennai 600117, India*
[2]*JNTUA College of Engineering Pulivendula, 516390, India*
[3]*Mumbai Educational Trust, Mumbai 400050, India*

ABSTRACT: In this proposed work, a miniaturized dual band-pass filter with enhanced selectivity and tunable transmission zero is proposed for an ISM and Sub-6 GHz application. The conventional open and short circuited stubs are employed to operate dual band resonance. This prototype consists of a Square Complementary Split Ring Resonator (SCSRR), a unit cell interdigital circuit, and short and open circuited stubs. Further, the selectivity of the filter is enhanced by employing the SCSSR on the ground plane of the filter. The D-CRL resonator consists of a set of interdigital lines that act as main section of the filter which provides dual band-pass filter at ISM and sub-6 GHz bands with the bandwidths of 0.3 GHz and 0.75 GHz, respectively. The experimentally validated filter has 39 and 59% 3-dB fraction bandwidths, maximum insertion losses on both the bands below 0.31 dB, passband impedance matching more than 31 dB, group delay in the range of 0.25 to 0.61 ns, stopband to passband selectivity 89 dB/GHz, and passband to stopband selectivity 93 dB/GHz. The presented dual-band prototype is a better candidate to use in ISM and sub-6 GHz spectrum based high speed digital communication.

1. INTRODUCTION

The contemporary wireless systems require optimum performance filters which could have adaptable center frequency (CFs), passband and stopband bandwidths, and abrupt rejection. Compact quad-band band-pass filters were implemented by employing stepped-impedance coupled-line quad-mode resonators (SICLQMRs) [1–4]. The novel design of ultra-wide band-pass filter is designed using ultra-wideband right/left-handed (CRLH) and uniplanar complementary split ring resonator (UP-CSRR). These types of filter designs are used in broad band applications reported in [5–8]. Miniaturized low-pass filter combining an asymmetric π-type microstrip line and a defect structure were used to achieve higher suppression and cost reduction [9]. A conductor-backed coplanar waveguide high-pass filter for satellite based applications (C-band) comprises a hexagonal resonator with interdigital coupling and a high impedance line fabricated in a coplanar by etching a square ring metallic pattern in the ground plane of the substrate [10–14]. A technical review on filtering antennas or filtennas realizes both the antenna and filter functions in a single configuration with the main idea of minimizing size and losses in the radio system design [15–18]. The transmission-line analysis and even-and-odd mode analysis are employed to analyze the frequency-response of an H-shaped slot resonator etched in the ground plane [19–22]. U-shape folded high impedance line using a microstrip low-pass filter was designed and analyzed with a conventional filter which characterizes a ripple less passband and improved stopband properties [23, 24].

The main aim of this analysis is proposing a dual-passband filter that resonates at ISM and sub-6 GHz spectrum with minimum insertion loss, high selectivity, and tunable transmission zeros in the passband. In order to achieve this, an interdigital line with two short and open circuited stubs are embedded. Also, two SCSRRs are printed on the bottom of the open circuited stubs to achieve circuit miniaturization and high selectivity in both the resonance bands namely passband to stopband slope and stopband to passband slope.

2. DUAL BAND FILTER DESIGN USING CIRCUIT AND MATRIX MODEL BASED ANALYSIS

The microstrip layout of the proposed prototype is designed and optimized by using a Rogers RT duroid 5880 based substrate with the electrical and physical dimension of height $\varepsilon_r = 2.2$, $\tan[\delta] = 0.002$ and $h = 0.708$ mm. The dual-band filter consists of open and short circuited stubs with an inter-digital coupled line on the power plane and SCSRR on the ground plane. In order to operate in the ISM and sub-6 GHz spectrum, a dual band-pass filter called an inter-digital coupled line with an integrated stub is employed. The inter-digital coupled-based resonator optimizes the upper passband transmission zeros in addition to resonating in two passbands. The selectivity of the filter is further enhanced by employing the SCSSR on the ground plane of the filter. Two SCSRRs are used in the filter design,

* Corresponding author: Thupalli Shaik Mahammed Basha (mahammadbasha.ece@jntua.ac.in).

doi:10.2528/PIERC24032705

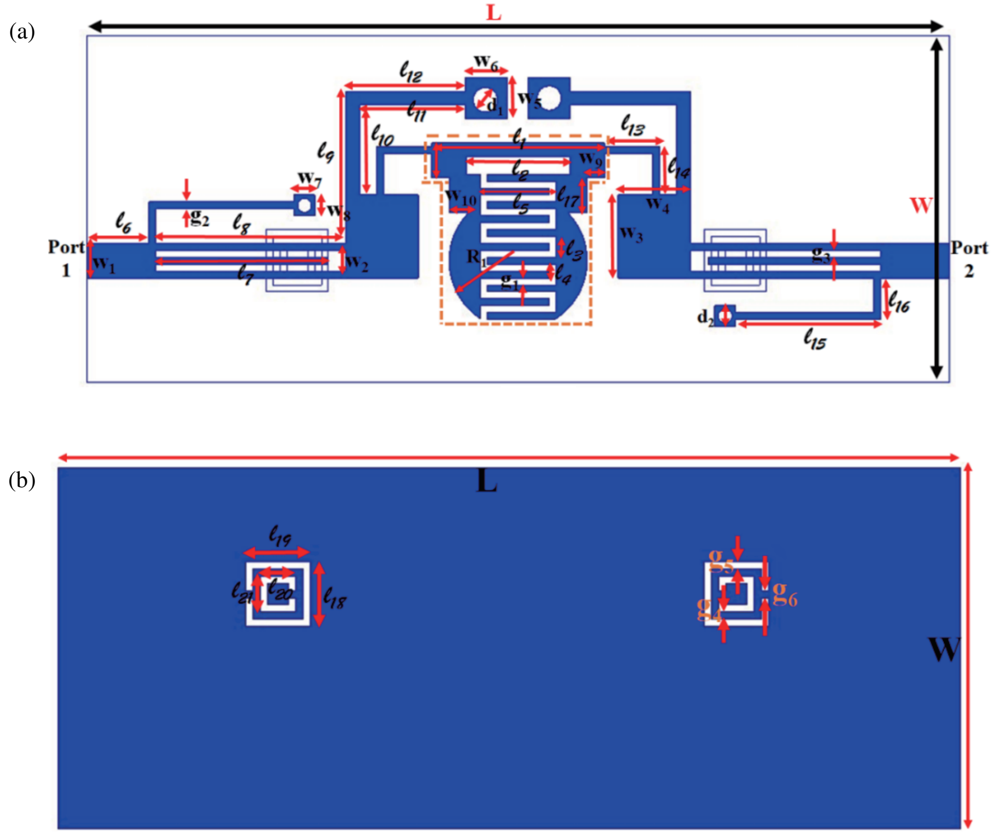

FIGURE 1. Proposed layout dual band pass filter structure. (a) Top view and (b) Bottom view.

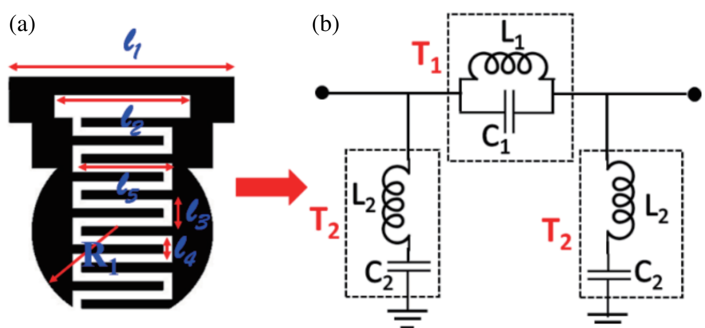

FIGURE 2. Interdigital coupled line unit cell: (a) Microstrip layout and (b) Approximate equivalent circuit model.

and both the SCSRRs are located beneath the input/output port interdigital line. For the proper optimization of the location and size of the SCSRR, the passband selectivity of the filter is 0.912. This is essential for sub-6 GHz applications bandwidth viability. This section calculates the scattering parameters for each component displayed in Fig. 1 as well as the filter's transfer function in the Laplace domain.

Figure 2 illustrates the inter-digital coupled circuit along with its corresponding lumped model. The parallel resonator, made up of L_1 and C_1, is shown in series with the main channel, and the parasitic series resonators, made up of L_2 and C_2, are shown on each side of the cell.

The interdigital capacitor C_1's estimated value in Fig. 2(b) may be computed using Equation (1) derived from [11].

$$C_1\left(pf\right) = \frac{\varepsilon_{reff}10^{-9}}{17\pi^2}\frac{M(m)}{M'(m)}\left(n-1\right)k_1 \tag{1}$$

where $M(m)$ and $M'(m)$ are elliptic functions constructed by [11]; K_1 stands for the finger width; n is the number of fingers; and ε_{re} is the effective dielectric constant.

$$\frac{M\left(m\right)}{m'\left(m\right)} = \frac{\pi}{Ln\left[\frac{2\left(1+\sqrt{m'}\right)}{1-\sqrt{m'}}\right]} \quad \text{for} \quad 0 \leq m \leq 0.707 \tag{2}$$

TABLE 1. The optimized physical dimension of the presented dual band-pass filter.

Parameter	mm	Parameter	mm	Parameter	mm	Parameter	mm
L_1	5	L_{20}	0.6	L_{12}	3.48	w_4	1.7
L_2	3	L_{21}	0.8	L_{13}	1.6	w_5	1.2
L_3	0.2	g_1	0.1	L_{14}	1.4	w_6	1.2
L_4	0.6	g_2	0.2	L_{15}	4.2	w_7	0.6
L_5	2	g_3	0.2	L_{16}	1.2	w_8	0.6
L_6	1.8	g_4	0.2	L_{17}	1	w_9	0.5
L_7	5	g_5	0.2	L_{18}	1.4	w_{10}	0.57
L_8	5.5	g_6	0.2	L_{19}	1.8	R_1	14
L_9	4.4	w_1	1	d_1	0.4	d_2	0.7
L_{10}	2.6	w_2	0.6	L	25	W	10
L_{11}	3.08	w_3	2.4	-	-	-	-

$$\frac{M(m)}{m'(m)} = \frac{1}{\pi} Ln\left[2\frac{1+\sqrt{m}}{1-\sqrt{m'}}\right] \quad \text{for} \quad 1 \geq m \geq 0.707 \tag{3}$$

where the definitions of the constants k and k_0 are

$$M = \tan^2\left(\frac{a\pi}{4b}\right), \quad a = \frac{w_1}{2} \quad \text{and} \quad b = \frac{w_1+s}{2} \tag{4}$$

$$M' = \sqrt{1-K^2} \tag{5}$$

It is necessary to specify the significance for L_1 in Fig. 2(b) in order to determine the cell's primary resonance frequency. L_1 may be computed as follows [12] since parallel microstrip line and interdigital capacitor are the approximate inductance values.

$$L_1\,(nH) = 2 \times 10^{-6} l_2 \left[\ln\left(\frac{l_2}{w_2+t}\right) + 1.193 + .2235\frac{w_2+t}{l_2}\right] \times M_g \tag{6}$$

where the microstrip line's thickness, length, and width are denoted by t, l_2, and w_2, respectively, and M_g is a modification constant that can be expressed as follows [12] and resembles how the ground layer affects the inductance value.

$$M_g = 0.57 - 0.145 \ln\left(\frac{w_1}{h}\right) \quad \text{for} \quad \frac{w_1}{h} > 0.05 \tag{7}$$

where w_1 denotes the microstrip line's width and h the substrate's thickness.

The values of L_2 and C_2 are determined from the resonant frequency response. Also, the proposed filter's resonant frequencies are compared with the simulated response (HFSS C 2021B) and equivalent circuit analysis. In Fig. 1, optimized lumped element values are listed in Table 1. The theory of microwave network is used to determine the filtering characteristics of the unit cell once the lumped elements were determined. The $ABCD$ matrix shown in Fig. 2(b) may be used to describe both series and parallel resonators [12]:

$$T_1 = \begin{pmatrix} 1 & (L_1 S)/(L_1 C_1 S^2 + 1) \\ 0 & 1 \end{pmatrix} \tag{8a}$$

$$T_2 = \begin{pmatrix} 1 & 0 \\ (C_2 S)/(C_2 L_2 S^2 + 1) & 1 \end{pmatrix} \tag{8b}$$

The complete inter-digital capacitor's $ABCD$ matrix may thus be expressed as follows:

$$T_{\text{D-CRLH CELL}} = T_2 \times T_1 \times T_2 = \begin{pmatrix} A_t & B_t \\ C_t & D_t \end{pmatrix} \tag{9}$$

As a result, the suggested cell's transfer function (S_{21}) and return loss (S_{11}) may be determined as [12].

$$S_{11} = \frac{\frac{A_t+B_t}{Z_0} - C_t Z_0 - D_t}{\frac{A_t+B_t}{Z_0} + C_t Z_0 + D_t} \tag{10a}$$

$$S_{11} = \frac{2}{\frac{A_t+B_t}{Z_0} + C_t Z_0 + D_t} \tag{10b}$$

The scattering characteristics of the inter-digital coupled line are demonstrated by inserting the matrix coefficients from (9) into (10a) and (10b), as illustrated in Fig. 3. From Fig. 3, it is detected that the frequency response of the inter-digital coupled line reveals that the first primary resonance occurs at 1 GHz, while the second resonance caused by the series resonator (L_2 and C_2) occurs at 3.25 GHz. Therefore, this inter-digital line acts as a dual band-pass filter at 2.4 GHz and 4.8 GHz with a wider stopband spectrum of 3 GHz. The lumped element and microstrip model of fixed stubs are connected in series with a central transmission line, which are accountable for improving lower band reflecting coefficient at 2.4 GHz, as illustrates in Fig. 4. The frequency response of this stub is optimized by tuning the stub length L, and it acts as a lower spectrum band-pass filter. The above mentioned stubs $ABCD$ matrix can be expressed by,

$$T_{embedded} = \begin{pmatrix} 1 & (LS)/\left(CLS^2+1\right) \\ 0 & 1 \end{pmatrix}$$

TABLE 2. Optimal values of grouped components for the filter's component sections and a streamlined representation of the presented filter.

Lumped Part	Inductor	Capacitor
Interdigital coupled line unit cell (Fig. 2(b))	$L_1 = 0.97\,\mathrm{nH}$	$C_1 = 0.430\,\mathrm{pF}$
Fixed stub (Fig. 4)	$L_2 = 1.14\,\mathrm{nH}$	$C_2 = 0.522\,\mathrm{pF}$
short-/Open-circuited stubs (Fig. 6(c))	$L = 0.764\,\mathrm{nH}$	$C = 0.197\,\mathrm{pF}$
	$L_1 = 3.5\,\mathrm{nH}$	$C_1 = 0.380\,\mathrm{pF}$
Simplified model (Fig. 7(b))	$L_2 = 1.67\,\mathrm{nH}$	$C_2 = 0.197\,\mathrm{pF}$
	$L_2 = 4.22\,\mathrm{nH}$	$C_1 = 0.920\,\mathrm{pF}$
	$L_4 = 3.11\,\mathrm{nH}$	$C_3 = 1.280\,\mathrm{pF}$
	$L_5 = 5.45\,\mathrm{nH}$	$C_5 = 0.215\,\mathrm{pF}$

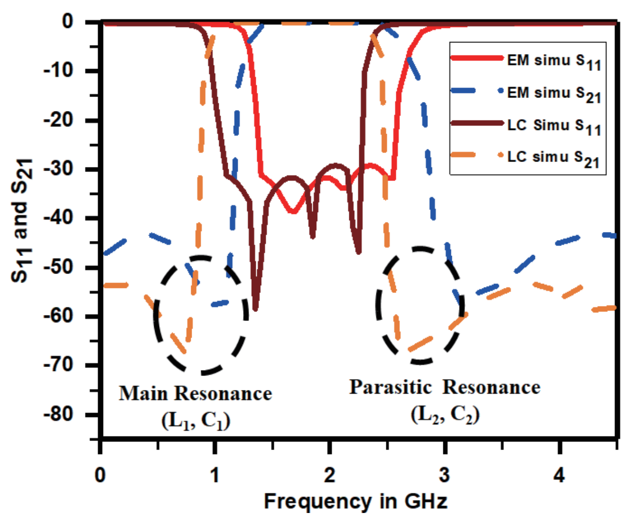

FIGURE 3. Interdigital coupled line unit cell equivalent circuit (EM and LC circuit simulation) scattering response.

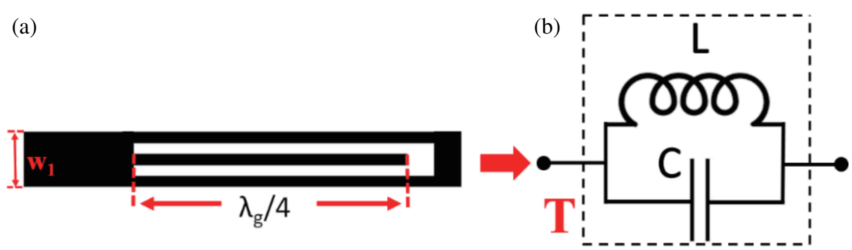

FIGURE 4. Open circuit stub laded microstrip line (a) microstrip line layout and (b) lumped circuit.

$$= \begin{pmatrix} A_t & B_t \\ C_t & D_t \end{pmatrix} \tag{11}$$

The scattering parameters are determined for various stub length (L) values by inserting matrix coefficients of (11) into (10a) and (10b), as illustrated in Fig. 5. The center narrow stopband frequency shifts to low values by increasing the L value. From Fig. 5, it is understood that the stub length L has better S_{21} response at 4 mm. Using the above optimization, the lower band-pass filter is identified as below 3 GHz spectrum. The center operating resonance frequency shifts towards the lower spectrum by increasing L value. From Fig. 4, it is observed that the optimized value of L to improve the upper band-pass filter is around 3 mm, which resonates around 3.2 GHz. Accordingly, the Ansys HFSS 2021B software was used to determine the necessary and optimized response for the lumped elements from Fig. 4, which are provided in Table 2. Transmission line theory is used to construct lumped models for these components, shown in Figs. 6(a) and 6(b). Thus, it is possible to determine lumped elements physical values from the short-circuited stub illustrated in Fig. 6(a). The

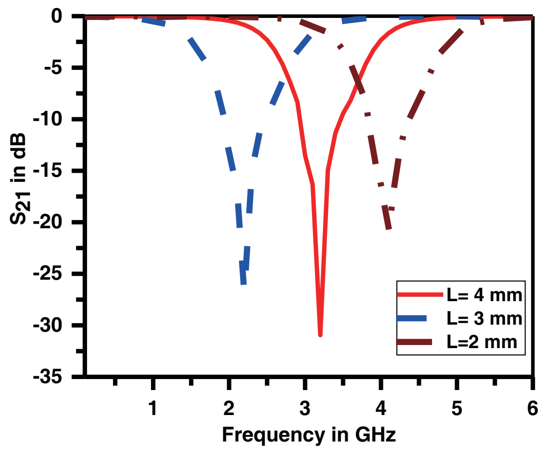

FIGURE 5. The S_{21} response with respect to different values of L.

transmission line input and the admittance from the lumped model are determined by using [13]:

$$C = \frac{(2n-1)\,Y_0\pi}{2\omega_0}, \quad L = \frac{1}{\omega_0^2 C} = \frac{4}{(2n-1)\,Y_0\pi} \tag{12}$$

where ω_0 is the angular frequency, and $Y_0 (= 1/Z_0)$ is the typical admittance. From Fig. 6(b), the open-circuited stubs are obtained by using the same methodology, and its physical lumped elements values are [15]

$$L = \frac{(2n-1)\,Z_0\pi}{4\omega_0}, \quad C = \frac{1}{\omega_0^2 L} = \frac{4}{(2n-1)\,Z_0\pi\omega_0} \tag{13}$$

The lumped and microstrip models for the parallel-connected short and open-circuited stubs are depicted in Fig. 6(c). By repeating the process from Eqs. (8a) and (8b), the proposed filter configuration $ABCD$ matrix can be expressed as,

$$T_1 = \begin{pmatrix} 1 & 0 \\ \left(L_1C_1S^2+1\right)/\left(L_1S\right) & 1 \end{pmatrix} \tag{14a}$$

As a result, the structure's overall $ABDC$ matrix is

$$T_2 = \begin{pmatrix} 1 & 0 \\ (C_2S)/(C_2L_2S^2+1) & 1 \end{pmatrix} \tag{14b}$$

$$T_{stub} = T_1 \times T_2 = \begin{pmatrix} A_t & B_t \\ C_t & D_t \end{pmatrix} \tag{15}$$

The lumped elements illustrated in Fig. 6(c) are derived using the HFSS equivalent circuit optimization and are listed in Table 2. The scattering parameters were derived by introducing the matrix coefficients of (15) into (10a) and (10b), and they are shown in Fig. 6(d), where strong transmission is observed from 5.5 GHz and 7.5 GHz, and a narrow stopband characteristics can be observed at 11.5 GHz. Fig. 7(a) introduces and illustrates a complete circuit lumped-element model which shows the circuit complexity of the model.

Parts I and II, which are concerned with the filter's out-of-band performance, can be avoided in order to simplify the model using Tee and Pi conversions and address this complexity while still investigating the passband characteristics. As a result, the simpler equivalent circuit model is illustrated in Fig. 7(b). The $ABCD$ matrix of each and every section illustrated in Fig. 7(b) is obtained by using the microwave network theory from [17]

$$T_1 = \begin{pmatrix} 1 & 0 \\ \left(C_3L_4S^2+1\right)/\left(L_4S\right) & 1 \end{pmatrix} \tag{16a}$$

$$T_2 = \begin{pmatrix} 1 & L_2S \\ 0 & 1 \end{pmatrix} \tag{16b}$$

$$T_3 = \begin{pmatrix} 1 & 0 \\ C_1S & 1 \end{pmatrix} \tag{16c}$$

$$T_4 = \begin{pmatrix} 1 & \left(L_4S\right)/\left(C_5L_6S^2+1\right) \\ 0 & 1 \end{pmatrix} \tag{16d}$$

Consequently, the $ABCD$ matrix for the summarized configuration is expressed as

$$T_t = T_1 \times T_2 \times T_3 \times T_4 \times T_3 \times T_2 \times T_1 = \begin{pmatrix} A_t & B_t \\ C_t & D_t \end{pmatrix} \tag{17}$$

Therefore, the return loss (S_{11}) and transfer function (S_{21}) for the simplified configuration are determined by applying final matrix coefficients from (18) and (19) into (10a) and (10b).

$$S_{21} = \frac{as(bS^2+1)}{cS^8+dS^7+eS^6+\ldots+f} \tag{18}$$

$$S_{11} = -\left(\frac{as^8+bs^6+Cs^4+ds^2+e}{gS^8+hS^7+kS^6+\ldots+m}\right) \tag{19}$$

The simulated S_{21} and S_{11} are compared with the calculated values from (18) and (19) as shown in Fig. 7(b). From the above comparison it is observed that the presented filter resonates at 2.4 GHz and 5.5 GHz, respectively.

3. FULL-WAVE ANALYSIS, FABRICATION, AND COMPARISON

A photograph of the fabricated filter is illustrated in Fig. 8 with an optimized dimension. Note that a compact filter is designed by coupling all of the parts (specified in Section 2) together before fabrication, as shown in Fig. 8. The constructed prototype filter's group delay ranges from 0.35 ns to 0.6 ns in both passbands. For several microwave applications, these values are in the acceptable range. Further, the filtering characteristics were analyzed using HFSS 2021B full-wave finite element method. The experimentally validated and numerically simulated filtering performances are compared and illustrated in Fig. 8. Also, this result shows a good agreement between the two passbands. The experimentally validated filter has lower and upper band impedance bandwidths of 9% and 17%, respectively. The measured result matches with full wave simulation result, and it is higher than the simulated result at 2.45 and 5.45 GHz, respectively.

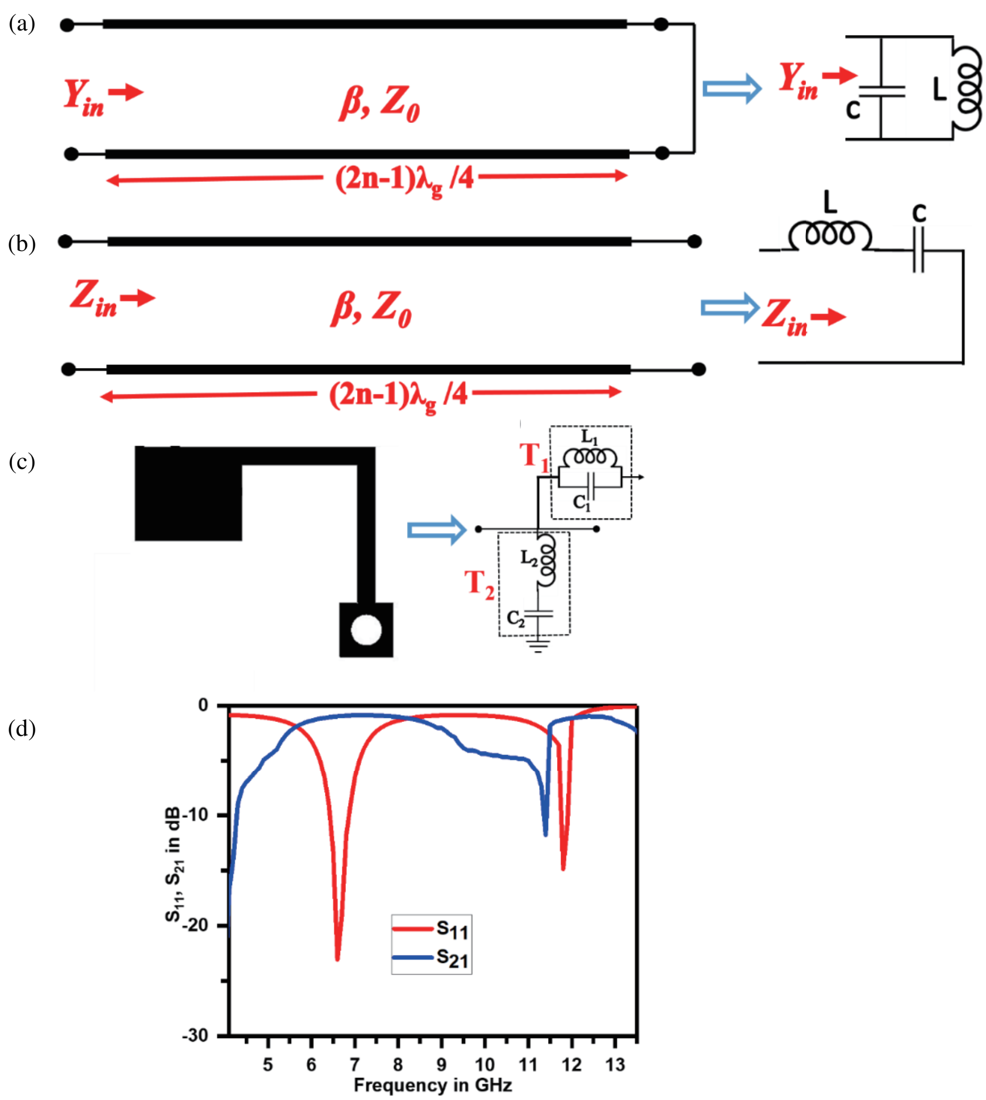

FIGURE 6. Equivalent circuit analysis of (a) transmission line with Short-circuited stubs and (b) transmission line with open-circuited stubs, (c) equivalent lumped model from microstrip configuration, and its (d) corresponding S-parameter response.

TABLE 3. Comparison of previously published work with the work that is being presented (IL: insertion loss, SIW: substrate integrated wave guide, BW: 3-dB fractional bandwidth).

Ref	Size (λ_g^2)	IL (dB)	3-dB BW%	Technique	Selectivity (dB/GHz)
[3]	0.87×0.91	0.91	37,42	Microstrip	12,36
[10]	1.29×0.39	0.61	36	SIW	23
[13]	1.1×0.49	0.89	31	Co-axial	36
[17]	1.22×0.55	0.53	51,37	SIW	17,29
[21]	0.39×1.12	0.49	22	Microstrip	45
Proposed	0.37×0.17	0.31	39, 59	Microstrip	89,93

Also, the proposed filter has an insertion loss below 0.31 dB in passband. The measured insertion loss was below 0.31 dB in both the passbands. As demonstrated in Fig. 8, the filter also has a high selectivity capability in both operating bands, from passband to stopband and from stopband to passband slope, which enhances electromagnetic suppression in the adjacent bands. The simulated group delay response is shown in Fig. 9. The proposed filter has lower and higher passband group delay val-

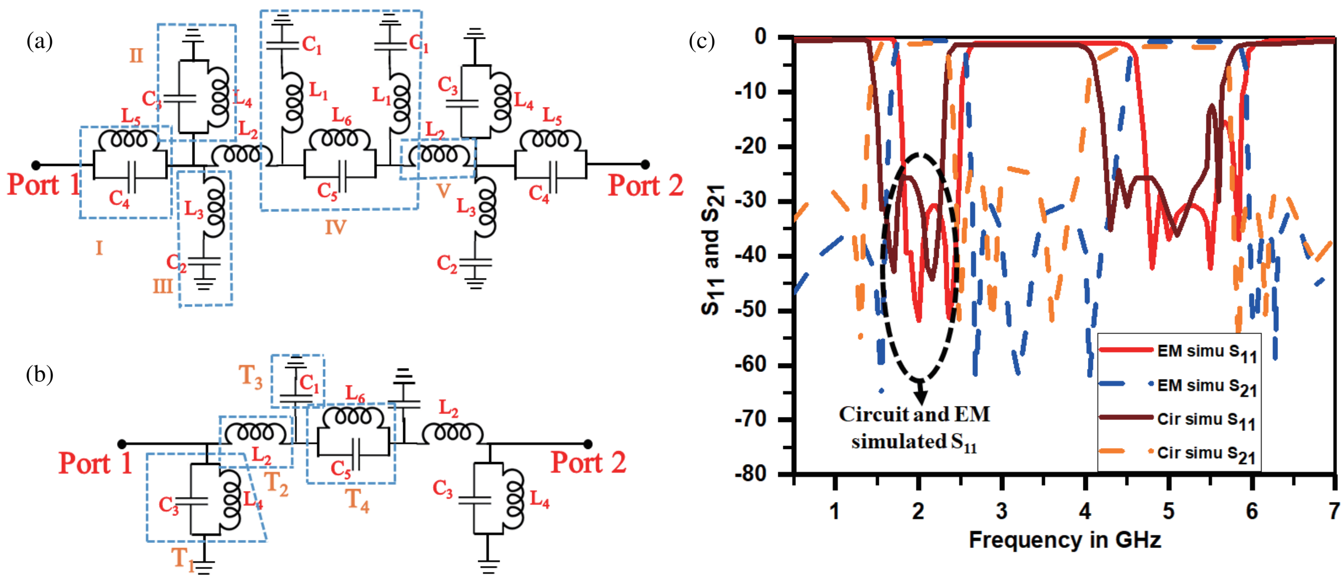

FIGURE 7. Proposed dual band pass filter's lumped parameter equivalent circuit models (a) detailed circuit model and (b) simplified two port equivalent circuit (c) EM and circuit simulated S_{11} and S_{21} response.

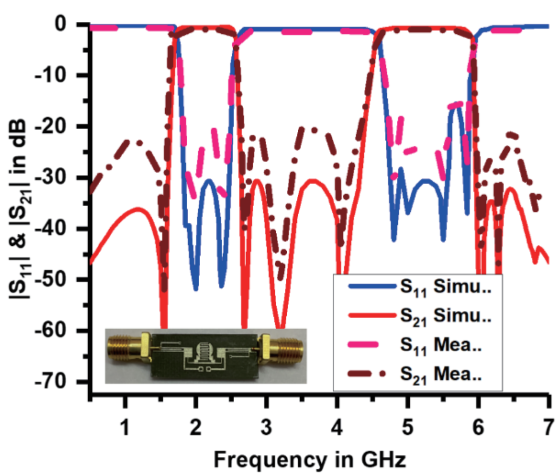

FIGURE 8. Photograph of the fabricated filter, simulated and measured S-parameters.

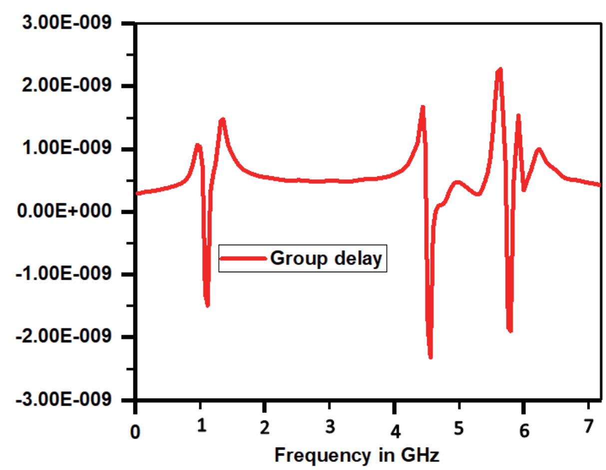

FIGURE 9. Proposed dual-band pass filter simulated group delay response.

ues of 2 ns and 2.3 ns, respectively. Finally, a comparison table of the proposed filter's filtering characteristics with recently reported articles and its significant enhancements are tabulated in Table 3.

4. CONCLUSION

In this article, a minimized, SCSSR loaded dual band-pass filter with a high selectivity is presented, fabricated, and analyzed. This phototype has low insertion loss with tunable multiple transmission zeros in both the passbands due to the close proximity transmission poles. Further, the selectivity of the filter is enhanced by employing the SCSSR on the ground plane of the filter. The D-CRL resonator consists of a set of interdigital lines which act as main section of the filter and provides dual band-pass filter at ISM and sub-6 GHz bands with the bandwidth of 0.3 GHz and 0.75 GHz, respectively. The experimentally validated filter has 39 and 59 % 3-dB fraction bandwidths, maximum insertion loss on both the bands below 0.31 dB, passband impedance matching more than 31 dB, group delay in the range of 0.25 to 0.61 ns, stopband to passband selectivity 89 dB/GHz, and the passband to stopband selectivity 93 dB/GHz. Due to the outstanding filtering characteristics and minimized size, the presented dual-band prototype is a good candidate to use in ISM and sub-6 GHz spectrum based high speed digital communication system.

REFERENCES

[1] Liu, Y., C. Tomassoni, S. Pei, and Y. Tian, "Compact quad-band band-pass filters using stepped-impedance coupled-line resonators," *International Journal of RF and Microwave Computer-Aided Engineering*, Vol. 30, No. 7, e22227, 2020.

[2] Abdalla, M. A., A. A. A. Aziz, and G. Arafa, "Novel configuration of ultra-wide band uni-planar configuration of complementary split ring resonator composite right/left-handed based band pass filter with sharp roll off and good stopband attenuation," *International Journal of RF and Microwave Computer-Aided Engineering*, Vol. 30, No. 11, e22400, 2020.

[3] Shi, L.-F., Z.-Y. Fan, and D.-j. Xin, "Miniaturized low-pass filter based on defected ground structure and compensated microstrip line," *Microwave and Optical Technology Letters*, Vol. 62, No. 3, 1093–1097, 2020.

[4] Souprayen, O. C. and T. Sadasivam, "Miniaturized conductor-backed CPW high-pass filter for C-band satellite applications," *Microwave and Optical Technology Letters*, Vol. 61, No. 6, 1478–1481, 2019.

[5] Bhardwaj, P., S. Deivalakshmi, and R. Pandeeswari, "Compact wideband substrate integrated waveguide bandpass filter for X/Ku-band application," *International Journal of RF and Microwave Computer-Aided Engineering*, Vol. 31, No. 6, e22634, 2021.

[6] Seyyed Najjar Hoseini, S. M., R. Zaker, and K. Monfaredi, "A microstrip folded compact wideband band-pass filter with wide upper stopband," *ETRI Journal*, Vol. 43, No. 6, 957–965, 2021.

[7] Gangwar, A. K., M. S. Alam, V. Rajpoot, and A. K. Ojha, "Filtering antennas: A technical review," *International Journal of RF and Microwave Computer-Aided Engineering*, Vol. 31, No. 10, e22797, 2021.

[8] Raoufi, T. and A. A. Heidari, "Compact low-pass/band-pass filters based on quarter-mode substrate integrated waveguide and a connected network of csrrs," *IET Microwaves, Antennas & Propagation*, Vol. 13, No. 12, 2177–2184, 2019.

[9] Sen, S. and T. Moyra, "Compact microstrip low-pass filtering power divider with wide harmonic suppression," *IET Microwaves, Antennas & Propagation*, Vol. 13, No. 12, 2026–2031, 2019.

[10] Zhang, T., F. Xiao, J. Bao, and X. Tang, "A compact UWB bandpass filter with a notched band using a multistubs loaded resonator," *International Journal of RF and Microwave Computer-Aided Engineering*, Vol. 27, No. 1, e21054, 2017.

[11] Killamsetty, V. K. and B. Mukherjee, "Compact dual bandpass filter for terrestrial radio and GSM applications," *International Journal of RF and Microwave Computer-Aided Engineering*, Vol. 27, No. 8, e21131, 2017.

[12] Wu, Y., Q. Zeng, and Y. Shang, "A low-insert loss and high-return loss bandpass filter based on cut-off rectangular waveguide for satellite communication application," *International Journal of RF and Microwave Computer-Aided Engineering*, Vol. 31, No. 2, e22351, 2021.

[13] Wang, C.-J. and L.-J. Hsu, "Design and analysis of a low-pass filter utilizing a slotted-ground-plane resonator," *Microwave and Optical Technology Letters*, Vol. 60, No. 4, 905–915, 2018.

[14] Rajput, A., K. Patel, and A. Birwal, "Compact microstrip low pass filter design using U-shaped folded high-impedance line," *Microwave and Optical Technology Letters*, Vol. 60, No. 7, 1812–1815, 2018.

[15] Pachaiyappan, G. and P. Ramanujam, "Design of low profile coaxial fed high gain stacked patch antenna for Wi-Fi/WLAN/Wi-Max applications," *Frequenz*, Vol. 75, No. 1-2, 27–34, 2021.

[16] Ramanujam, P., K. Ramanujam, and M. Ponnusamy, "A novel asymmetrical interdigital coupled line-based penta-band bandpass filter design with enhanced selectivity employing square complementary split ring resonator," *International Journal of RF and Microwave Computer-Aided Engineering*, Vol. 31, No. 12, e22888, Aug. 2021.

[17] Wei, F., C. Y. Zhang, C. Zeng, and X. W. Shi, "A reconfigurable balanced dual-band bandpass filter with constant absolute bandwidth and high selectivity," *IEEE Transactions on Microwave Theory and Techniques*, Vol. 69, No. 9, 4029–4040, Sep. 2021.

[18] Senthilkumar, S., U. Surendar, P. Ramanujam, and J. William, "A dual-polarized metamaterial spiral MIMO antenna for 5G applications," *Applied Physics A*, Vol. 128, No. 7, 607, 2022.

[19] Ramanujam, P., P. G. R. Venkatesan, M. Ponnusamy, and T. K. Sethuramalingam, "Design of miniaturized dual-band filtering antenna with improved selectivity utilizing square complementary split ring resonator for 5G MM-wave automobile applications," *International Journal of RF and Microwave Computer-Aided Engineering*, Vol. 32, No. 11, e23378, 2022.

[20] Sambathkumar, P., K. Ramanujam, and P. Ramanujam, "Design of 6×2 linear feed antenna array with suppressed SLL by employing CCSRR for Ka-band and 5G mm-wave applications," *Applied Physics A*, Vol. 129, No. 4, 287, 2023.

[21] Raoufi, T. and A. A. Heidari, "Compact low-pass/band-pass filters based on quarter-mode substrate integrated waveguide and a connected network of CSRRs," *IET Microwaves, Antennas & Propagation*, Vol. 13, No. 12, 2177–2184, 2019.

[22] Sen, S. and T. Moyra, "Compact microstrip low-pass filtering power divider with wide harmonic suppression," *IET Microwaves, Antennas & Propagation*, Vol. 13, No. 12, 2026–2031, 2019.

[23] Gangwar, A. K., M. S. Alam, V. Rajpoot, and A. K. Ojha, "Filtering antennas: A technical review," *International Journal of RF and Microwave Computer-Aided Engineering*, Vol. 31, No. 10, e22797, 2021.

[24] Zhao, X.-B., F. Wei, P. F. Zhang, and X. W. Shi, "Mixed-mode magic-Ts and their applications on the designs of dual-band balanced out-of-phase filtering power dividers," *IEEE Transactions on Microwave Theory and Techniques*, Vol. 71, No. 9, 3896–3905, Sep. 2023.